

# FTIR study of the products of the reaction between HCCO and NO

U. Eickhoff and F. Temps\*

Institut für Physikalische Chemie, Universität Kiel, Olshausenstr. 40, D-24098 Kiel, Germany.  
E-mail: temps@phc.uni-kiel.de

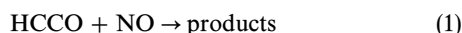
Received 17th September 1998, Accepted 16th November 1998

The main pathways of the reaction  $\text{HCCO} + \text{NO} \rightarrow \text{products}$  (1) were investigated at room temperature in the gas phase in Ar at 570 mbar pressure by employing FTIR spectroscopy. Mixtures of  $\text{NO}_2\text{-C}_2\text{H}_2\text{-NO-Ar}$  were photolysed under stationary conditions using a high-pressure Hg lamp at  $\lambda = 312$  nm. HCCO was generated in the reaction system in the reactions  $\text{NO}_2 + h\nu \rightarrow \text{O}(^3\text{P}) + \text{NO}$ ,  $\text{O}(^3\text{P}) + \text{C}_2\text{H}_2 \rightarrow \text{H} + \text{HCCO}$ . The main products of reaction (1) include  $\text{CO}_2$ ,  $\text{CO}$ , and  $\text{HCNO}$ . The results can be rationalised with the reaction channels  $\text{HCCO} + \text{NO} \rightarrow \text{HCN} + \text{CO}_2$  (1a) and  $\text{HCCO} + \text{NO} \rightarrow \text{HCNO} + \text{CO}$  (1d). The branching ratios were determined to be  $k_{1a}/k_1 = (0.28 \pm 0.10)$  and  $k_{1d}/k_1 = (0.64 \pm 0.12)$ . Formation of  $\text{HNCO}$  could not be confirmed. Other species detected include  $\text{H}_2\text{O}$  and  $\text{HONO}$ . These are formed, together with additional  $\text{CO}$ , in consecutive reactions of H atoms and OH radicals.

## 1 Introduction

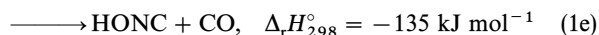
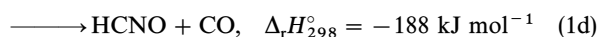
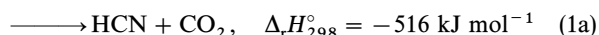
Elucidation of the mechanisms of NO reburning processes in flames is of great interest because of their importance for reducing the emission of  $\text{NO}_x$  from hydrocarbon combustion (see *e.g.* ref. 1–4 and references therein). However, rather little is known about many of the elementary chemical reactions which may participate.

The reaction



is assumed to play a key role in NO reburning, especially in fuel-rich flames (see *e.g.* ref. 5 and 6). Reaction (1) is known to be rather fast under room-temperature conditions ( $k_1 = 1.8 \times 10^{13} \text{ cm}^3 \text{ mol}^{-1} \text{ s}^{-1}$ ).<sup>7–9</sup> However, the product distribution and the detailed mechanism are not well understood.<sup>9,10</sup> In particular, there are many thermodynamically allowed product channels,<sup>11–14</sup> including:

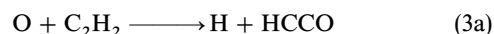
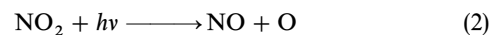
HCCO + NO



The reaction is generally assumed to proceed *via* complex formation.  $\text{HC(NO)CO}$ , nitrosoketene, can be formed at high pressures as a collisionally stabilized recombination product. On the other hand, in the low-pressure regime, the initially formed complex can dissociate *via* several exit channels. The yields of HCN *vs.* the different possible isomeric ‘‘HCON’’ species and the branching ratios between these isomers are of considerable relevance for modelling  $\text{NO}_x$  reburning.<sup>15–17</sup>

Here, we report results of a recent study of reaction (1) which allowed us to identify the main product channels of the reaction and to determine their branching ratios. The investigation involved photolysis of mixtures of  $\text{NO}_2\text{-C}_2\text{H}_2\text{-NO-Ar}$

and product analysis by FTIR spectroscopy. The HCCO radicals were produced in the reaction system *via* the reaction sequence:



The paper is organized as follows: Following this Introduction, Section 2 summarizes the experimental details. Section 3 describes the experimental results which were obtained. This section is divided into three subsections: The first reports the results of the qualitative and quantitative product measurements, the second describes the reaction mechanism which provides a basis for rationalizing the data, and the third presents the results for the branching ratio of the reaction. Section 4 contains a discussion of the experimental data, numerical simulations of the reactions system, comparisons with other experimental and theoretical investigations, and a brief discussion of implications of the measurements for the NO reburning mechanism. The main conclusions are gathered in Section 5.

## 2 Experimental

The title reaction was studied in a 21.3 cm long, 4.6 cm id, Duran glass reaction cell sealed with NaCl windows. The set-up was similar to that described in our study of the reaction of  $\text{CH}_2$  with  $\text{NO}$ .<sup>18</sup> The cell was situated in the sample chamber of an FTIR spectrometer (IFS 66V, Bruker) and connected to an all-glass vacuum system for gas handling, evacuated by a turbomolecular pump. Gas mixtures,  $\text{NO}_2\text{-C}_2\text{H}_2\text{-NO-Ar}$ , were prepared manometrically in a storage bulb. Care was taken to allow sufficient time for mixing. The mixtures were then transferred to the reaction cell, where they were photolysed with light from a 200 W high-pressure Hg lamp (Oriol). The Hg light spectrum was narrowed by using a 300–340 nm, 45° reflective dielectric mirror as a bandpass filter. The resulting photolysis spectrum was dominated by the strong 312 nm Hg line. The Hg light was collimated and imaged into the reaction cell with the dielectric mirror in order to irradiate the entire reaction volume as evenly as possible.

FTIR spectra were taken with  $0.25\text{ cm}^{-1}$  nominal resolution by co-adding 100 scans. A weak Norton–Beer apodization function was used and a zero-filling factor of 8. Strong IR absorption lines were chosen for the quantitative determinations of the different molecules of interest, in order to achieve high detection sensitivities with minimal interferences from other species in the reaction mixtures. The absorption line profiles were integrated using the standard OPUS software supplied with the spectrometer. Reference spectra of calibrated gas mixtures of the pure substances in Ar were used for converting the integrated IR signals to corresponding partial pressures. Gas mixtures for the calibrations were prepared systematically for each species, with concentrations in ranges similar to those found in the reaction to take into account deviations from the Lambert–Beer law at the spectrometer resolution used.

All gases used were of the highest commercially available purities: Ar (99.9999%),  $\text{C}_2\text{H}_2$  (99.6%),  $\text{NO}_2$  (98%), NO (99.5%), CO (99.997%), and  $\text{CO}_2$  (99.995%). Ar, CO, and  $\text{CO}_2$  were taken as supplied.  $\text{C}_2\text{H}_2$ ,  $\text{NO}_2$ , and NO were carefully purified until no impurities could be detected in their FTIR spectra.  $\text{C}_2\text{H}_2$ ,  $\text{NO}_2$ , and NO were condensed in traps at 77 K and purified until no impurities could be detected in their FTIR spectra.  $\text{C}_2\text{H}_2$  and NO were condensed in traps at 77 K and purified by fractional distillation. The first fraction of the  $\text{C}_2\text{H}_2$ , which evaporated upon slowly warming, was free of acetone; the first tenth of the evaporated NO was free of NO and  $\text{N}_2\text{O}$ . HCNO for measuring FTIR reference spectra was synthesised by pyrolysis of 3-phenyl-4-oxoiminoisoxazol-5-(4H)-one.<sup>19</sup> Reference samples of HCN and HNCO were prepared by heating mixtures of NaCN or NaNCO with stearic acid. HONO was obtained as a 1 : 1 mixture with  $\text{NH}_3$  in equilibrium over solid  $\text{NH}_4\text{NO}_2$ .<sup>20</sup>

### 3 Results

#### 3.1 Reaction products

The investigation of reaction (1) began with qualitative and quantitative measurements of the products of the photolysis of a series of different  $\text{NO}_2$ – $\text{C}_2\text{H}_2$ –NO–Ar gas mixtures in the reaction cell. The partial pressures of the gases were adjusted to maximize the effect of reaction (1) on the observable reaction products. All mixtures contained *ca.* 0.15 mbar  $\text{NO}_2$  and *ca.* 30 mbar  $\text{C}_2\text{H}_2$ . The NO was systematically varied from  $0 \leq p_{\text{NO}}/\text{mbar} \leq 20$ . A constant total pressure of *ca.* 570 mbar was reached by adding Ar. The exact mixture compositions are listed in Table 1. The total photolysis times were 60 min. FTIR spectra were taken before (reaction time “zero”) and, with the Hg light blocked for the duration of the FTIR scans, after 5, 10, 20, 40, and 60 min irradiation. Further spectra

were taken up to 240 min after the photolysis in order to check for possible dark reactions which could deplete reaction products. No sign of a dark reaction was observed before the start of the photolysis, even after storing a reactant mixture for up to 24 h.

A typical FTIR “product” spectrum is depicted in Fig. 1. This was obtained with a reaction mixture of 0.147 mbar  $\text{NO}_2$ , 29.61 mbar  $\text{C}_2\text{H}_2$ , and 4.93 mbar NO in Ar at 569.1 mbar total pressure (mixture 11, see Table 1) after a photolysis time of 60 min. A spectrum taken immediately before the photolysis was subtracted from the measured 60 min spectrum to obtain the difference spectrum shown. The different molecules were identified with the help of reference spectra, depicted in Fig. 1 for comparison underneath the product spectrum. All molecules which are depleted are shown with negative signals

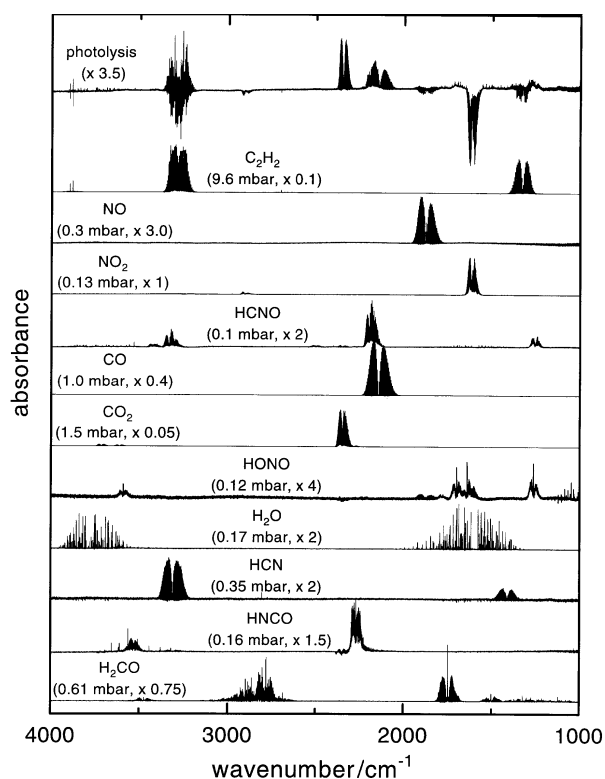


**Fig. 1** FTIR spectra. Top trace: Measured difference spectrum (“product spectrum”) for mixture 11 (Table 1) after 60 min photolysis. A spectrum taken immediately before the photolysis was subtracted from the measured 60 min spectrum to obtain the difference spectrum shown. Species which are depleted are shown with negative signals, while products exhibit positive signals. Below: Reference spectra of the different pure gases for comparison.

**Table 1** Experimental conditions, product yields (60 min photolysis), and branching ratios  $\Gamma_{\text{CO}_2}$ ,  $\Gamma_{\text{CO}}$ , and  $\Gamma_{\text{HCNO}}$  for the different  $\text{NO}_2$ – $\text{C}_2\text{H}_2$ –NO–Ar mixtures. The quoted average values were derived from mixtures 5–13.

Mixture number	$p_{\text{total}}/\text{mbar}$	$p_{\text{NO}_2}/\text{mbar}$	$p_{\text{C}_2\text{H}_2}/\text{mbar}$	$p_{\text{NO}}/\text{mbar}$	$-\Delta p_{\text{NO}_2}/\text{mbar}$	$p_{\text{CO}_2}/\text{mbar}$	$p_{\text{CO}}/\text{mbar}$	$p_{\text{HCNO}}/\text{mbar}$	$\Gamma_{\text{CO}_2}$	$\Gamma_{\text{CO}}$	$\Gamma_{\text{HCNO}}$
1	572.5	0.146	30.56	0.00	0.1339	0.0158	0.0322	0.0131	0.29	0.35	—
2	569.5	0.151	29.98	0.45	0.1136	0.0108	0.0340	0.0213	0.24	0.50	0.26
3	564.9	0.149	29.78	0.92	0.1040	0.0122	0.0360	0.0243	0.29	0.61	0.37
4	575.6	0.148	30.03	1.48	0.0954	0.0110	0.0331	0.0240	0.28	0.61	0.41
5	560.9	0.151	29.70	1.86	0.0934	0.0117	0.0323	0.0218	0.31	0.61	0.37
6	571.2	0.153	30.12	2.24	0.0881	0.0099	0.0320	0.0233	0.28	0.65	0.44
7	564.5	0.153	30.39	2.45	0.0958	0.0108	0.0334	0.0251	0.28	0.61	0.43
8	579.5	0.153	29.87	2.50	0.0853	0.0100	0.0319	0.0233	0.29	0.68	0.47
9	572.8	0.152	30.53	3.07	0.0835	0.0095	0.0301	0.0221	0.28	0.63	0.44
10	571.6	0.151	30.00	3.96	0.0751	0.0095	0.0278	0.0205	0.31	0.66	0.45
11	569.1	0.147	29.61	4.93	0.0770	0.0120	0.0314	0.0212	0.38	0.74	0.45
12	572.8	0.154	30.48	10.17	0.0525	0.0078	0.0238	0.0180	0.35	0.82	0.60
13	572.7	0.148	30.47	19.95	0.0352	0.0053	0.0136	0.0137	0.34	0.62	0.66
Av.	570.0	0.150	30.00	0–20	—	—	—	—	$0.31 \pm 0.10$	$0.67 \pm 0.12$	$0.48^{+0.25}_{-0.12}$

(NO<sub>2</sub> and NO), while products exhibit positive signals. The spectra were integrated and converted to partial pressures and concentrations to obtain reactant and product time profiles.

The main reaction products were CO<sub>2</sub>, CO, and HCNO. These products are seen in Fig. 2 which shows an expanded part (from 2400 to 2000 cm<sup>-1</sup>) of the spectrum of Fig. 1. The CO<sub>2</sub> and CO absorptions are immediately obvious. The production of HCNO could be unambiguously seen from the observed characteristic  $\nu_2$ ,  $\nu_2 + \nu_5 - \nu_5$ , and  $\nu_2 + \nu_4 - \nu_4$  IR band systems at 2125–2230 cm<sup>-1</sup>.<sup>21</sup> The HCNO absorption lines overlapped with the somewhat stronger CO R branch lines in the same region, but single rovibrational lines could be found to determine both species. Despite its strong IR absorption around 2275 cm<sup>-1</sup>, a region without other interfering absorptions, HCNO could not be detected. Thus, HCNO does not appear to be a product of reaction (1). HCN, the assumed co-product of the observed CO<sub>2</sub> from reaction (1a), was also not detected in the FTIR spectra. However, the HCN absorption band at 1400 cm<sup>-1</sup> is relatively weak, while the bands around 725 and 3300 cm<sup>-1</sup> were obscured by the strong C<sub>2</sub>H<sub>2</sub> absorptions. C<sub>2</sub>H<sub>2</sub> was always present in very large excess; its pressure was too high to allow analysis of the C<sub>2</sub>H<sub>2</sub> depletion because of the small change during the reaction.

In addition to the above-mentioned main products, HONO and H<sub>2</sub>O were observed (*cf.* Fig. 1). However, these two molecules are not of major interest in the following. Very weak additional FTIR absorption signals were observed at around 1775 and 1795 cm<sup>-1</sup> and still remain to be assigned; the respective molecules can be only very minor products.

Measured reactant and product time profiles for a selected measurement (mixture 10; 0.151 mbar NO<sub>2</sub>, 30.0 mbar C<sub>2</sub>H<sub>2</sub>, 3.96 mbar NO, 571.6 mbar total pressure) are plotted in Fig. 3. The NO<sub>2</sub> depletion reaches *ca.* 50% after 60 min photolysis. Correspondingly, the products CO<sub>2</sub>, CO, and HCNO as well as HONO and H<sub>2</sub>O increased with time, as expected. The

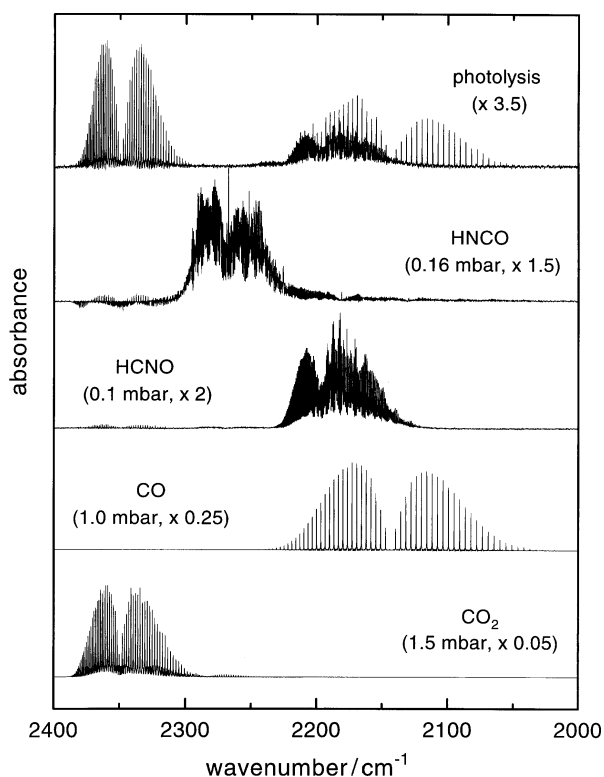


**Fig. 2** Part of Fig. 1 (mixture 11) on an expanded scale, showing the formation of the reaction products CO<sub>2</sub>, CO, and HCNO. The product spectrum is given by the top trace, different reference spectra are shown underneath. Note the absence of HCNO in the product spectrum.

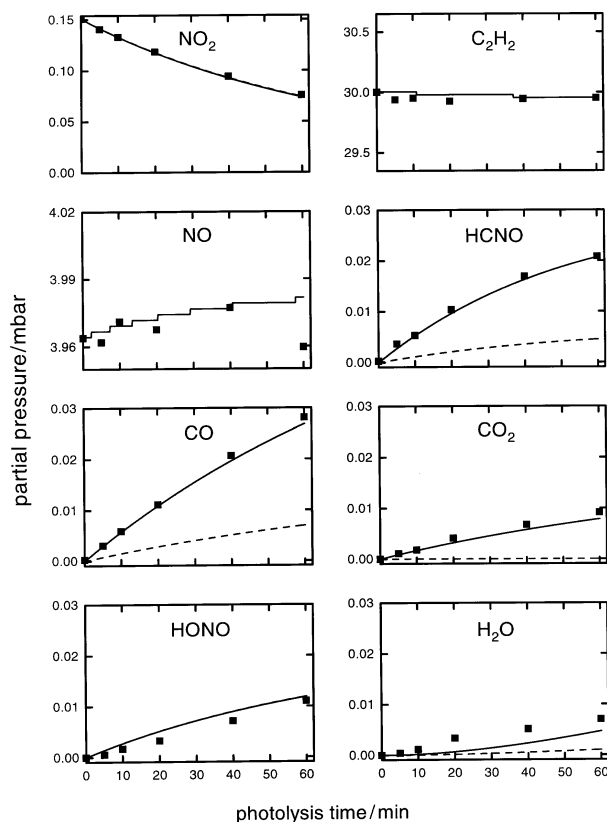


**Fig. 3** Measured reactant and product partial pressures as a function of photolysis time (mixture 10, Table 1). Filled symbols show the experimental data, full lines refer to the results of the numerical simulations (see Discussion).

C<sub>2</sub>H<sub>2</sub> and NO, which were present in large excess, remained practically constant. Analogous plots were obtained for the other reaction mixtures.

Comparing the data from all experimental runs, the total NO<sub>2</sub> consumption was found to decrease from *ca.* 90% after 60 min photolysis in the measurement without added NO to *ca.* 25% at  $p_{\text{NO}} = 20$  mbar. The production of CO<sub>2</sub> and CO was seen to decrease correspondingly. Despite the drop in the total NO<sub>2</sub> consumption, the absolute yield of HCNO was found to exhibit (at first) a pronounced increase upon addition of increasing NO, before decreasing again due to the smaller total NO<sub>2</sub> consumption. A maximum of HCNO formation was observed in the measurement with  $p_{\text{NO}} = 2.45$  mbar. This trend shows the importance of reaction (1d) for the product formation.

After completion of the photolysis, the NO<sub>2</sub>, NO, CO<sub>2</sub>, and CO remained constant. Measurements of the HCNO after photolysis showed a weak decay under the conditions in the reaction cell, due to a slow (presumably heterogeneous) dark reaction. However, an effect on the branching ratio for reaction (1) can be eliminated by considering the initial product formation rates at short photolysis times (see below). A slow decay was also seen for HONO, while H<sub>2</sub>O, being a product of the HCNO and HONO decomposition steps, was seen to increase slowly.

The measured absolute NO<sub>2</sub> depletions and the corresponding CO<sub>2</sub>, CO, and HCNO product yields after 60 min photolysis are compiled in Table 1. In addition, Table 2 lists the initial NO<sub>2</sub> depletion rates and the corresponding initial product formation rates determined from the observed time profiles towards short reaction times.

### 3.2 Reaction mechanism

The reaction mechanism which provides a basis for rationalising the observed product yields consists of (i) the NO<sub>2</sub> photolysis system, (ii) the reactions involving HCCO radicals,

**Table 2** Initial product formation rates and resulting branching ratios  $\Gamma_{\text{CO}_2}$ ,  $\Gamma_{\text{CO}}$ , and  $\Gamma_{\text{HCNO}}$  determined for the different  $\text{NO}_2\text{-C}_2\text{H}_2\text{-NO-Ar}$  mixtures. The quoted average values were derived from mixtures 5–13.

Mixture number	$p_{\text{total}}/\text{mbar}$	$p_{\text{NO}_2}/\text{mbar}$	$p_{\text{C}_2\text{H}_2}/\text{mbar}$	$p_{\text{NO}}/\text{mbar}$	$-r_{\text{NO}_2}^0/\text{mbar min}^{-1}$	$r_{\text{CO}_2}^0/\text{mbar min}^{-1}$	$r_{\text{CO}}^0/\text{mbar min}^{-1}$	$r_{\text{HCNO}}^0/\text{mbar min}^{-1}$	$\Gamma_{\text{CO}_2}$	$\Gamma_{\text{CO}}$	$\Gamma_{\text{HCNO}}$
1	572.5	0.146	30.56	0.00	0.008 37	0.000 90	0.001 43	0.000 50	0.27	0.17	—
2	569.5	0.151	29.98	0.45	0.003 50	0.000 30	0.000 93	0.000 60	0.21	0.41	0.22
3	564.9	0.149	29.78	0.92	0.003 03	0.000 33	0.000 97	0.000 73	0.27	0.55	0.39
4	575.6	0.148	30.03	1.48	0.002 50	0.000 29	0.000 90	0.000 77	0.29	0.64	0.55
5	560.9	0.151	29.70	1.86	0.002 43	0.000 29	0.000 90	0.000 79	0.30	0.67	0.59
6	571.2	0.153	30.12	2.24	0.002 38	0.000 22	0.000 83	0.000 71	0.23	0.61	0.53
7	564.5	0.153	30.39	2.45	0.002 55	0.000 26	0.000 83	0.000 75	0.25	0.55	0.51
8	579.5	0.153	29.87	2.50	0.002 32	0.000 22	0.000 77	0.000 80	0.24	0.57	0.64
9	572.8	0.152	30.53	3.07	0.002 07	0.000 17	0.000 77	0.000 68	0.20	0.66	0.59
10	571.6	0.151	30.00	3.96	0.001 87	0.000 19	0.000 63	0.000 65	0.25	0.57	0.64
11	569.1	0.147	29.61	4.93	0.001 72	0.000 23	0.000 69	0.000 62	0.32	0.72	0.66
12	572.8	0.154	30.48	10.17	0.001 23	0.000 14	0.000 53	0.000 45	0.27	0.77	0.65
13	572.7	0.148	30.47	19.95	0.000 70	0.000 09	0.000 25	0.000 28	0.29	0.55	0.69
Av.	570.0	0.150	30.00	0–20	—	—	—	—	$0.26 \pm 0.10$	$0.63 \pm 0.10$	$0.61 \pm 0.14$

including their formation in the reaction  $\text{O} + \text{C}_2\text{H}_2$  and their subsequent depletion, especially *via* reaction (1), (iii) reactions of  $\text{CH}_2$  radicals which are formed in the second channel of the  $\text{O} + \text{C}_2\text{H}_2$  reaction, and (iv) reactions of H atoms and OH radicals and additional consecutive reactions. The different elementary reactions and the rate constants taken into account are compiled in Table 3. The main reactants for the various radical species are  $\text{NO}_2$ , NO, and  $\text{C}_2\text{H}_2$ , which are present in the reaction mixtures in much higher concentrations than all other species.

**3.2.1 Photolysis of  $\text{NO}_2$ .** The photolysis of  $\text{NO}_2$  has been studied in considerable detail in a number of laboratories (see *e.g.* ref. 12 and 22–24). The photodissociation of  $\text{NO}_2$  in the

300–340 nm wavelength region leads to  $\text{O}(^3\text{P})$  atoms,



with a quantum yield of unity.<sup>12,22,23</sup> However, recombination of the O atoms with NO and their reaction with  $\text{NO}_2$  have to be taken into account,



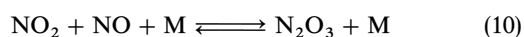
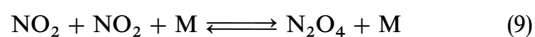
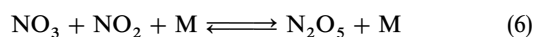
Reactions (4) and (5b) are in the low-pressure regime under the conditions used. The respective rate constants are well

**Table 3** Elementary reactions in the detailed reaction mechanism

Reaction	$k/\text{cm}^3 \text{mol}^{-1} \text{s}^{-1} \text{ }^{a-c}$	Ref.
$\text{HCCO} + \text{NO} \rightarrow \text{HCN} + \text{CO}_2$ (1a)	$5.0 \times 10^{12}$	This work
$\text{HCCO} + \text{NO} \rightarrow \text{HCNO} + \text{CO}$ (1d)	$1.3 \times 10^{13}$	This work
$\text{NO}_2 + h\nu \rightarrow \text{NO} + \text{O}$ (2)	$1.3 \times 10^{-4} \text{ }^{a,c}$	See Text
$\text{O} + \text{C}_2\text{H}_2 \rightarrow \text{H} + \text{HCCO}$ (3a)	$6.4 \times 10^{10}$	26–29
$\text{O} + \text{C}_2\text{H}_2 \rightarrow \text{}^3\text{CH}_2 + \text{CO}$ (3b)	$1.6 \times 10^{10}$	26–29
$\text{O} + \text{NO} + \text{M} \rightarrow \text{NO}_2 + \text{M}$ (4)	$5.5 \times 10^{11} \text{ }^b$	12, 25
$\text{O} + \text{NO}_2 \rightarrow \text{NO} + \text{O}_2$ (5a)	$5.8 \times 10^{12}$	12
$\text{O} + \text{NO}_2 + \text{M} \rightarrow \text{NO}_3 + \text{M}$ (5b)	$7.4 \times 10^{11} \text{ }^b$	12
$\text{NO}_3 + \text{NO}_2 + \text{M} \rightarrow \text{N}_2\text{O}_5 + \text{M}$ (6)	$6.3 \times 10^{11} \text{ }^b$	12
$\text{N}_2\text{O}_5 + \text{M} \rightarrow \text{NO}_3 + \text{NO}_2 + \text{M}$ (–6)	$4.2 \times 10^{-2} \text{ }^a$	12
$\text{NO}_3 + \text{NO} \rightarrow \text{NO}_2 + \text{NO}_2$ (7)	$1.6 \times 10^{13}$	12
$\text{NO}_3 + \text{O} \rightarrow \text{NO}_2 + \text{O}_2$ (8)	$1.0 \times 10^{13}$	12
$\text{NO}_2 + \text{NO}_2 + \text{M} \rightarrow \text{N}_2\text{O}_4 + \text{M}$ (9)	$8.3 \times 10^9 \text{ }^b$	12
$\text{N}_2\text{O}_4 + \text{M} \rightarrow \text{NO}_2 + \text{NO}_2 + \text{M}$ (–9)	$6.0 \times 10^4 \text{ }^a$	12
$\text{NO}_2 + \text{NO} + \text{M} \rightarrow \text{N}_2\text{O}_3 + \text{M}$ (10)	$1.9 \times 10^9 \text{ }^b$	12
$\text{N}_2\text{O}_3 + \text{M} \rightarrow \text{NO}_2 + \text{NO} + \text{M}$ (–10)	$1.5 \times 10^5 \text{ }^a$	12
$\text{HCCO} + \text{NO}_2 \rightarrow \text{HCNO} + \text{CO}_2$ (11a)	$8.0 \times 10^{12} \text{ }^{b,d}$	8
$\text{HCCO} + \text{NO}_2 \rightarrow \text{CO} + \text{other products}$ (11b)	$8.0 \times 10^{12} \text{ }^{b,d}$	8
$\text{HCCO} + \text{C}_2\text{H}_2 \rightarrow \text{products}$ (12)	$\leq 6 \times 10^9$	8
$\text{HCNO} \rightarrow \text{products}$ (13)	$1.0 \times 10^{-4} \text{ }^a$	See text
$\text{}^3\text{CH}_2 + \text{NO} \rightarrow \text{HCNO} + \text{H}$ (14a)	$1.9 \times 10^{13}$	18, 30
$\text{}^3\text{CH}_2 + \text{NO} \rightarrow \text{HCN} + \text{OH}$ (14b)	$3.3 \times 10^{12}$	18, 30
$\text{}^3\text{CH}_2 + \text{NO}_2 \rightarrow \text{products}$ (15)	$5.9 \times 10^{13}$	30
$\text{}^3\text{CH}_2 + \text{C}_2\text{H}_2 \rightarrow \text{products}$ (16)	$1.7 \times 10^8$	31
$\text{H} + \text{NO} + \text{M} \rightarrow \text{HNO} + \text{M}$ (17)	$3.2 \times 10^{11} \text{ }^b$	29, 32
$\text{H} + \text{NO}_2 \rightarrow \text{OH} + \text{NO}$ (18)	$8.0 \times 10^{13}$	28
$\text{H} + \text{C}_2\text{H}_2 + \text{M} \rightarrow \text{C}_2\text{H}_3 + \text{M}$ (19)	$1.0 \times 10^{11} \text{ }^b$	28
$\text{OH} + \text{NO} + \text{M} \rightarrow \text{HONO} + \text{M}$ (20)	$3.6 \times 10^{12} \text{ }^b$	12
$\text{OH} + \text{NO}_2 + \text{M} \rightarrow \text{HNO}_3 + \text{M}$ (21)	$3.5 \times 10^{12} \text{ }^b$	12
$\text{OH} + \text{C}_2\text{H}_2 + \text{M} \rightarrow \text{C}_2\text{H}_2\text{OH} + \text{M}$ (22)	$4.7 \times 10^{11} \text{ }^b$	12, 28, 29
$\text{C}_2\text{H}_2\text{OH} + \text{NO} \rightarrow \text{products}$ (23)	$5.0 \times 10^{12}$	Estimated
$\text{C}_2\text{H}_3\text{OH} + \text{NO}_2 \rightarrow \text{products}$ (24)	$5.0 \times 10^{12}$	Estimated

<sup>a</sup> First-order rate constant in  $\text{s}^{-1}$ . <sup>b</sup> Second-order rate constant in low pressure or fall-off regime in  $\text{cm}^3 \text{mol}^{-1} \text{s}^{-1}$  ( $\text{M} = \text{Ar}$ ,  $p = 570$  mbar). <sup>c</sup> Fitted effective first-order rate constant describing the  $\text{NO}_2$  photolysis. <sup>d</sup> Branching ratio adjusted to describe the measured formation of HCNO without added NO.

known (ref. 12, 24 and 25; see Table 3). Other consecutive reactions, *e.g.*



cannot have a significant effect on the observed final product distribution.<sup>12,23,24</sup> The small equilibrium amount ( $\leq 1\%$  of the  $\text{NO}_2$  at the highest  $\text{NO}$ ) of  $\text{N}_2\text{O}_3$  in the  $\text{NO}_2$ - $\text{NO}$  mixtures can be taken into account.

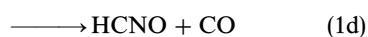
**3.2.2 Formation and depletion reactions of HCCO.** The HCCO radicals which are the subject of this work are produced in the reaction



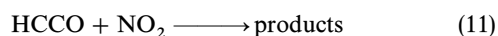
The branching ratios for (3a) and (3b) are known from measurements of the HCCO channel by Peeters and co-workers<sup>26</sup> and from a determination of the  $\text{CH}_2$  channel from our laboratory<sup>27</sup> to be  $k_{3a}/k_3 = 0.8$  and  $k_{3b}/k_3 = 0.2$  (each with estimated uncertainties of  $\pm 0.1$ ;  $k_3 = 8.0 \times 10^{10} \text{ cm}^3 \text{ mol}^{-1} \text{ s}^{-1}$ <sup>28,29</sup>). Hence, reaction (3a), *i.e.* production of HCCO, constitutes the main pathway, while  $\text{CH}_2$  formation is only of secondary importance.  $\text{CH}_2$  is generated in its  $\tilde{\text{X}}^3\text{B}_1$  ground electronic state ( $\equiv {}^3\text{CH}_2$ ).

The fraction of the O atoms leading to HCCO in the present work is given by  $k_{3a}[\text{C}_2\text{H}_2]/(k_3[\text{C}_2\text{H}_2] + k_4[\text{NO}] + k_5[\text{NO}_2])$ . Thus, under the conditions used, only between 59% (at  $p_{\text{NO}} = 0$ ) and 13% ( $p_{\text{NO}} = 20$  mbar) of the O atoms from the  $\text{NO}_2$  photolysis produce HCCO. A rather large fraction of the O atoms ( $k_4[\text{NO}]/(k_3[\text{C}_2\text{H}_2] + k_4[\text{NO}] + k_5[\text{NO}_2])$ ); up to *ca.* 76% at  $p_{\text{NO}} = 20$  mbar, the highest  $p_{\text{NO}} = 20$  mbar, the highest  $p_{\text{NO}}$ ) reacts *via* recombination with NO [reaction (4)]. However, reaction (4) is effectively a “zero cycle” reaction because it leads back to the  $\text{NO}_2$ . The reaction is only responsible for the observed reduction of the  $\text{NO}_2$  consumption in the experiments with increasing  $p_{\text{NO}}$ . Reaction (5) plays only a small role in the O atom balance. Hence, reactions (2) and (3a) constitute a suitable source for HCCO for the present purpose.

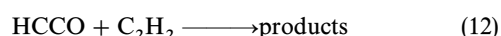
The subsequent HCCO depletion in the reaction system in the presence of a large excess of NO is dominated by the title reaction ( $k_1 = 1.8 \times 10^{13} \text{ cm}^3 \text{ mol}^{-1} \text{ s}^{-1}$ ).<sup>7-9</sup> From the experimentally observed formation of  $\text{CO}_2$ , CO, and HCNO, the reaction channels (1a) and (1d) are seen to constitute the main pathways,



Other HCCO reactions cannot compete with reaction (1) under all experimental conditions except at very low NO, where the reaction

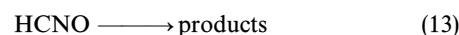


(with  $k_{11} = 1.6 \times 10^{13} \text{ cm}^3 \text{ mol}^{-1} \text{ s}^{-1}$ )<sup>8</sup> contributes to the product formation. It is worth noticing here that the product measurements in the absence of added NO indicate that reaction (11) can, at least in part, also produce HCNO. The reaction



(with  $k_{12} \leq 6 \times 10^9 \text{ cm}^3 \text{ mol}^{-1} \text{ s}^{-1}$ )<sup>8</sup> is too slow to play a role.

The slow HCNO decay reaction observed after photolysis could be formally described by a first-order reaction

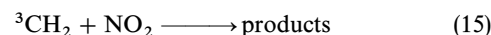


with an effective rate coefficient of  $k_{13} = (5.3 \pm 1.0) \times 10^{-5} \text{ s}^{-1}$  for all experimental runs.

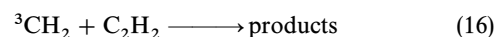
**3.2.3 Reactions of  $\text{CH}_2$ .** Additional reactions which have to be taken into account arise because of the formation of  ${}^3\text{CH}_2$  radicals in reaction (3b). The fast reaction



contributes to the production of HCNO (see ref. 18 and 30). However, the branching ratios for the two channels are known ( $k_{14a}/k_{14} = 0.84$  and  $k_{14b}/k_{14} = 0.15$ ).<sup>18</sup> The reaction



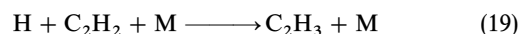
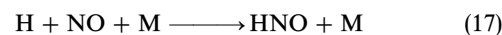
again can be important only at very low  $\text{NO}$ ,<sup>30</sup> while the reaction



is very slow<sup>31</sup> at room temperature.

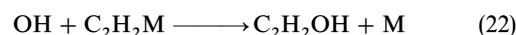
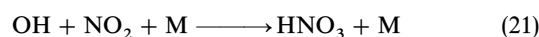
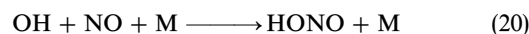
The production of HCNO *via* reaction (14a) in addition to reaction (1d) has to be taken into account to determine the branching ratio of reaction (1).

**3.2.4 Reactions of H atoms and OH radicals.** Further attention has to be directed to additional radical species which are produced in the reaction system. In particular, reaction (3a) leads to a corresponding amount of H atoms. Under the conditions used, the H atoms undergo consecutive reactions with NO,  $\text{NO}_2$ , and  $\text{C}_2\text{H}_2$ :



The respective reaction rate constants are well known (ref. 28, 29 and 32; see Table 3). With the rate constants as listed, the fractions of the H atoms reacting *via* the different routes  $\{k_{17}[\text{NO}]/(k_{17}[\text{NO}] + k_{18}[\text{NO}_2] + k_{19}[\text{C}_2\text{H}_2]) \text{ etc.}\}$  under the experimental conditions with  $p_{\text{NO}}$  in the range 0–20 mbar are 0–30%, 78–55%, and 22–15%, respectively, for the reactions with NO,  $\text{NO}_2$ , and  $\text{C}_2\text{H}_2$ .

The HNO from reaction (17) can undergo reactions with itself<sup>33</sup> or with  $\text{NO}_2$ . Likewise, the  $\text{C}_2\text{H}_3$  radicals from reaction (19) are likely to react with NO, either to give  $\text{C}_2\text{H}_2 + \text{HNO}$  or *via* recombination to  $\text{H}_2\text{CCHNO}$  (or  $\text{H}_2\text{CCNOH}$ , after subsequent isomerization). However, these consecutive reactions cannot affect the observed product distribution for reaction (1). The implications of the formation of OH radicals in reaction (18), on the other hand, need to be examined in a little more detail. The OH radicals undergo corresponding consecutive reactions with NO,  $\text{NO}_2$  and  $\text{C}_2\text{H}_2$ :



Reactions (20)–(22) are in their fall-off regimes under the conditions of interest. Taking the known rate constants (ref. 12, 28 and 29; see Table 3), the fractions of the OH reacting *via* the three different routes under the experimental conditions ( $p_{\text{NO}} = 0$ –20 mbar) are 0–83%, 4–1%, and 96–16% with NO,  $\text{NO}_2$ , and  $\text{C}_2\text{H}_2$ , respectively. Thus, while HONO has indeed been measured,  $\text{HNO}_3$  formation can be neglected. On the

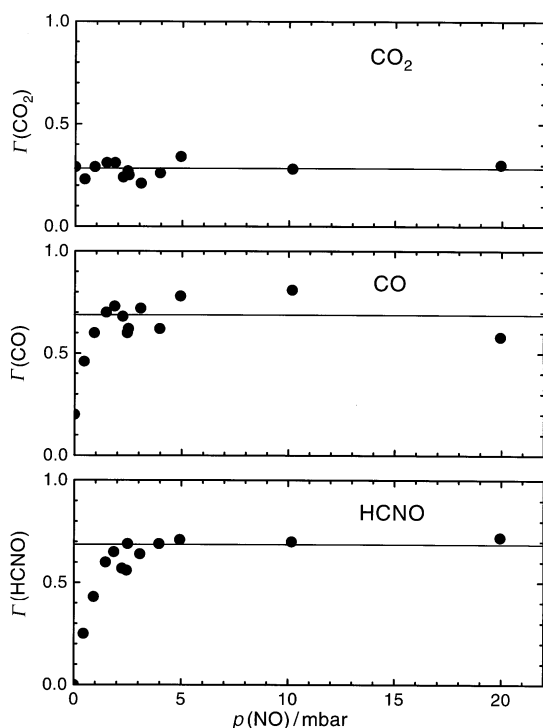
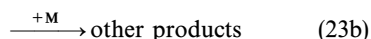
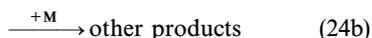
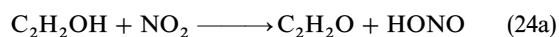


**Fig. 4** Measured yields of  $\text{CO}_2$ ,  $\text{CO}$ , and  $\text{HCNO}$  from reaction (1) as a function of the partial pressures of  $\text{NO}$  in the reaction mixtures.

other hand, it is seen that reaction (22) is the main  $\text{OH}$  depletion route at low  $\text{NO}$ , but it has only a small effect at high  $\text{NO}$ . This conclusion is important, since the  $\text{C}_2\text{H}_2\text{OH}$  complex from reaction (22) might react further with  $\text{NO}$ . Plausible reaction channels could include pathways



A recombination reaction (23b) would lead to stable molecules (*e.g.*  $\text{HOCH}=\text{CHNO}$ ,  $\text{HOCH}=\text{CNOH}$ ,  $\text{OCH}-\text{CHNOH}$ ,  $\text{c-C}_2\text{H}_3\text{NO}_2$ ), but reaction (23a) would be an unwanted additional  $\text{HCNO}$  source. As seen above, this extra source does not play an important role at high  $\text{NO}$ . Furthermore, it is pointed out that  $\text{H}_2\text{CO}$ , which is the second product of reaction (23a), could not be found, despite a detection sensitivity comparable to that for  $\text{HCNO}$ . Thus, reaction (23a) was neglected. A reaction according to



was taken into account to explain the observed  $\text{HONO}$  in the measurements without added  $\text{NO}$ .

### 3.3 Branching ratios for reactions (1a) and (1d)

The experimental data show that reaction (1) proceeds *via* the channels  $\text{HCCO} + \text{NO} \rightarrow \text{HCN} + \text{CO}_2$  (1a) and  $\text{HCCO} + \text{NO} \rightarrow \text{HCNO} + \text{CO}$  (1d). It is the task, in the following, to determine the branching ratios  $\Gamma_{1a} = k_{1a}/k_1$  and  $\Gamma_{1d} = k_{1d}/k_1$  for these two pathways.

Considering the above mechanism, at high  $\text{NO}$ , the reaction system is dominated by reactions (1)–(5a), (14), and (17)–(19). Under these conditions,  $\text{NO}_2$  depletion and  $\text{CO}_2$ ,  $\text{CO}$ , and  $\text{HCNO}$  production can be described with the rate equations

$$-r_{\text{NO}_2} = -\text{d}[\text{NO}_2]/\text{dt} = k_2 I_{\text{P}}[\text{NO}_2] - k_4[\text{NO}][\text{O}] + k_{18}[\text{NO}_2][\text{H}] \quad (1a)$$

$$r_{\text{CO}_2} = \text{d}[\text{CO}_2]/\text{dt} = k_{1a}[\text{NO}][\text{HCCO}] \quad (1b)$$

$$r_{\text{CO}} = \text{d}[\text{CO}]/\text{dt} = k_{1d}[\text{NO}][\text{HCCO}] + k_{3b}[\text{C}_2\text{H}_2][\text{O}] \quad (1c)$$

$$r_{\text{HCNO}} = \text{d}[\text{HCNO}]/\text{dt} = k_{1d}[\text{NO}][\text{HCCO}] + k_{14a}[\text{NO}][^3\text{CH}_2] \quad (1d)$$

where  $k_2 I_{\text{P}}[\text{NO}_2]$  is the effective  $\text{NO}_2$  photolysis rate under the experimental conditions. With the steady-state approximations for  $[\text{O}]$ ,  $[\text{H}]$ ,  $[\text{HCCO}]$ , and  $[^3\text{CH}_2]$ , and with the abbreviations

$$A = \frac{k_{3a}[\text{C}_2\text{H}_2]}{k_3[\text{C}_2\text{H}_2] + k_{5a}[\text{NO}_2]}$$

$$B = \frac{k_{18}[\text{NO}_2]}{k_{17}[\text{NO}] + k_{18}[\text{NO}_2] + k_{19}[\text{C}_2\text{H}_2]}$$

and

$$C = \frac{A}{1 + AB}$$

the branching ratios  $k_{1a}/k_1$  and  $k_{1d}/k_1$  are related to the experimental product yields according to

$$\frac{\text{d}[\text{CO}_2]}{-\text{d}[\text{NO}_2]} = \left( C \frac{k_{1a}}{k_1} \right) \quad (IIa)$$

$$\frac{\text{d}[\text{CO}]}{-\text{d}[\text{NO}_2]} = \left( C \frac{k_{1d}}{k_1} \right) + \frac{k_{3b}}{k_{3a}} \quad (IIb)$$

$$\frac{\text{d}[\text{HCNO}]}{-\text{d}[\text{NO}_2]} = \left( C \frac{k_{1d}}{k_1} \right) + \frac{k_{3b} k_{14a}}{k_{3a} k_{14}} \quad (IIc)$$

Here, the factors  $C = A/(1 + AB)$  in eqn. (IIa)–(IIc) simply account for the extra  $\text{NO}_2$  depletion routes *via* the reactions  $\text{O} + \text{NO}_2$  (5a) and  $\text{H} + \text{NO}_2$  (14), while the extra terms on the righthand sides in eqn. (IIb) and (IIc) allow for the additional  $\text{CO}$  and  $\text{HCNO}$  production routes  $\text{O} + \text{C}_2\text{H}_2 \rightarrow ^3\text{CH}_2 + \text{CO}$  (3b) and  $^3\text{CH}_2 + \text{NO} \rightarrow \text{HCNO} + \text{H}$  (14a).

Eqn. (IIa)–(IIc) are readily solved and evaluated. Thus, taking the experimental data as listed in Table 1, branching ratios  $\Gamma_{\text{CO}_2}$ ,  $\Gamma_{\text{CO}}$ , and  $\Gamma_{\text{HCNO}}$  (where, ideally,  $\Gamma_{\text{CO}_2}$  is identified with  $\Gamma_{1a}$  and  $\Gamma_{\text{CO}}$ ,  $\Gamma_{\text{HCNO}}$  with  $\Gamma_{1d}$ ) were found for the production of  $\text{CO}_2$ ,  $\text{CO}$ , and  $\text{HCNO}$ , respectively. The data for the different reaction mixtures are given in Table 1. Taking the points from the experimental runs with  $p_{\text{NO}} \geq 1.5$  mbar, the average values from the observed final product yields were found to be:  $\Gamma_{\text{CO}_2} = 0.31 \pm 0.10$ ,  $\Gamma_{\text{CO}} = 0.67 \pm 0.12$  and  $\Gamma_{\text{HCNO}} = 0.48 \pm 0.25$ . The error limits include the statistical and estimated systematical uncertainties.

Considering the slow  $\text{HCNO}$  decay reaction (13) observed after completion of the photolysis, the above  $\Gamma_{\text{HCNO}}$  value must, in fact, be considered as a lower limit to  $\Gamma_{1d}$ . This is reflected by the fact that  $\Gamma_{\text{HCNO}} < \Gamma_{\text{CO}}$  above. Obviously, reaction (13) has to be taken into account. This was accomplished by analysis of the initial  $\text{NO}_2$  depletion rates and the respective initial product formation rates determined at short reaction times. The initial rates which were determined from the different experimental time profiles (*e.g.* Fig. 3) have been collected in Table 2. The individual measurements were evaluated by using eqn. (IIa)–(IIc) above. The results, which are listed in Table 2, are plotted as a function of the  $\text{NO}$  pressures in the reaction mixtures in Fig. 4. The product branching ratios from the initial reaction rates including estimated systematical errors were found to be

$$\Gamma_{\text{CO}_2} = 0.26 \pm 0.10$$

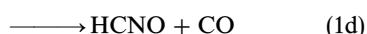
$$\Gamma_{\text{CO}} = 0.63 \pm 0.12$$

$$\Gamma_{\text{HCNO}} = 0.61 \pm 0.16$$

## 4 Discussion

### 4.1 Branching ratios for reactions (1a) and (1d)

According to the present measurements, the reaction between  $\text{HCCO}$  and  $\text{NO}$  has two main channels, *i.e.*



The production of CO, HCNO, and CO<sub>2</sub> was directly observed in the FTIR spectra. HCN was not detected because of the presence of high amounts of C<sub>2</sub>H<sub>2</sub>, but it is expected to be produced in conjunction with the CO<sub>2</sub> in reaction (1a).

The branching ratios for reactions (1a) and (1d) could be determined from the final product yields after completion of photolysis and from the initial product formation rates determined at short reaction times. The respective results are found to be in good agreement, if allowance is made for the slow heterogeneous decay of HCNO, which cannot be avoided. The final values for  $\Gamma_{\text{CO}}$  and  $\Gamma_{\text{HCNO}}$  agree with their experimental accuracies. This observation is very important, since one could imagine other sources for CO in the reaction system, whereas the possibilities for production of HCNO are very limited. The reaction  ${}^3\text{CH}_2 + \text{NO}$  (14a) gives only a small contribution, which was taken into account, and an effect of a reaction like  $\text{C}_2\text{H}_2\text{OH} + \text{NO} \rightarrow \text{HCNO} + \text{H}_2\text{CO}$  (23a) could be ruled out by the absence of H<sub>2</sub>CO.

Taking the average of the two  $\Gamma_{\text{CO}_2}$  values, the branching ratio for channel (1a) at room temperature and pressures around 570 mbar is found to be  $k_{1a}/k_1 = (0.28 \pm 0.10)$ . Likewise, taking the average of the two  $\Gamma_{\text{CO}}$  values and the  $\Gamma_{\text{HCNO}}$  value from the initial HCNO rise, the branching ratio for channel (1d) for the same conditions is  $k_{1d}/k_1 = (0.64 \pm 0.12)$ . According to eqn. (IIb) and (IIc), this value is somewhat dependent on the branching ratio for reactions (3a) and (3b). The above value was derived by adopting  $k_{3a}/k_3 = 0.8$ .<sup>26,27</sup> A smaller value for  $k_{3a}/k_3$  would lead to a smaller result for  $k_{1d}/k_1$  and a correspondingly higher value for  $k_{1a}/k_1$ . The quoted uncertainty limits refer to the 95% confidence level and include estimated systematic errors.

The above branching ratios add up to  $(k_{1a} + k_{1d})/k_1 = 0.92$ . Thus, within the experimental accuracy ( $\pm 0.10$ ), reactions (1a) and (1d) can account almost fully for the reaction. Some room ( $\leq 0.08$ ) is still left for small contributions from other reaction channels, including a collisional stabilization of the HCCO + NO association complex. Furthermore, one has to note that formation, *via* reaction (1e), of HONC, which would rapidly isomerize to HCNO, may not be excluded from the experimental data (it would be included in  $\Gamma_{\text{HCNO}}$ ). However, HOCN formation appears less likely considering the available information on the potential-energy hypersurface for the reaction (see below and ref. 10).

## 4.2 Simulations of the reaction system and sensitivity analysis

Numerical simulations of the reaction system were carried out in order to check the data analysis and investigate the effects of the different elementary steps which can play a role. The elementary reactions and rate constants taken into account are listed in Table 3. Fig. 3 includes the results of the simulations for one experimental run ( $p_{\text{NO}} = 3.96$  mbar; mixture 10, *cf.* Table 1). As seen, the experimental NO<sub>2</sub>, CO<sub>2</sub>, CO, and HCNO profiles are described very well. Similar agreement was observed for the different other reaction mixtures.

Also shown in Fig. 3 are simulated profiles obtained with  $k_1$  (and  $k_{1d}$ ) set to zero (dashed curve). Setting  $k_1 = 0$ , the production of CO<sub>2</sub> is turned off. Likewise, reactions (3b) and (14a) would remain as the sole sources for CO and HCNO, respectively. Neither reaction can account for the observed products. Thus, the calculated profiles give a clear demonstration of the importance of reactions (1a) and (1d) for the observed products. The simulations were less satisfactory for HONO and H<sub>2</sub>O, even though the trends in these profiles were predicted. However, these species did not enter into the analysis. They are consecutive products which could also be affected by heterogeneous reactions.

The importance of the individual elementary steps in the full reaction mechanism was further examined with a sensitivity analysis. The results of the sensitivity analysis for mixture 10 (time profiles for Fig. 3) are depicted in Fig. 5. Histograms of the reduced sensitivity coefficients  $\partial \ln c_i / \partial \ln k_j$  for HCNO, CO, and CO<sub>2</sub> for the main reaction steps are shown. As seen, the absolute yields of these products are most strongly affected by the NO<sub>2</sub> photolysis rate (2), the reaction  $\text{O} + \text{C}_2\text{H}_2$  (3), and the reaction  $\text{O} + \text{NO} + \text{M}$  (4), as well as the title reaction (1). The sensitivity coefficients for the three products with respect to reactions (2)–(5a) are very similar, which means that these reactions are of high importance only for the absolute product yields, not for the relative product amounts. The relative yields of CO<sub>2</sub> and CO and HCNO are seen to be determined by the ratio of the rate constants  $k_{1a}/k_{1d}$ .

## 4.3 Comparison with previous work

The overall rate constant for reaction (1) has been determined in three previous investigations. The reaction was first measured by direct means with detection of HCCO by IR diode laser absorption spectroscopy by Unfried *et al.*<sup>7</sup> HCCO radicals were generated in their study by photodissociation of CH<sub>2</sub>CO with an excimer laser at  $\lambda = 193$  nm. From the exponential HCCO decay curves at different NO concentrations, a rate constant value of  $k_1 = 2.3 \times 10^{13} \text{ cm}^3 \text{ mol}^{-1} \text{ s}^{-1}$  was found. The second investigation, by Temps *et al.*<sup>8</sup> employed the discharge flow technique with HCCO detection by laser magnetic resonance spectroscopy. The radical source was reaction (3), as in the present work. The measured rate constant value of  $k_1 = 1.3 \times 10^{13} \text{ cm}^3 \text{ mol}^{-1} \text{ s}^{-1}$  was somewhat lower than that of Unfried *et al.*<sup>7</sup> In any case, however, the reaction was confirmed to be very fast. In the third study, Boullart *et al.*<sup>9</sup> investigated the C<sub>2</sub>H<sub>2</sub>-O-NO system using the discharge flow-molecular beam mass spectrometry technique. These authors derived a room temperature value of  $k_1 = 1.8 \times 10^{13} \text{ cm}^3 \text{ mol}^{-1} \text{ s}^{-1}$  by following the change in steady-state mass signals of HCCO upon adding increasing amounts of NO. Further measurements up to 700 K did give indications for a small, but statistically significant, non-zero activation energy.<sup>9</sup>

The product branching ratio of reaction (1) has, to the best of our knowledge, been the subject of only one previous experimental study. In their mass spectrometric work cited above,<sup>9</sup> Boullart *et al.* examined the formation of CO and CO<sub>2</sub> produced in channels (1a)–(1e) at 700 K and 2 mbar.

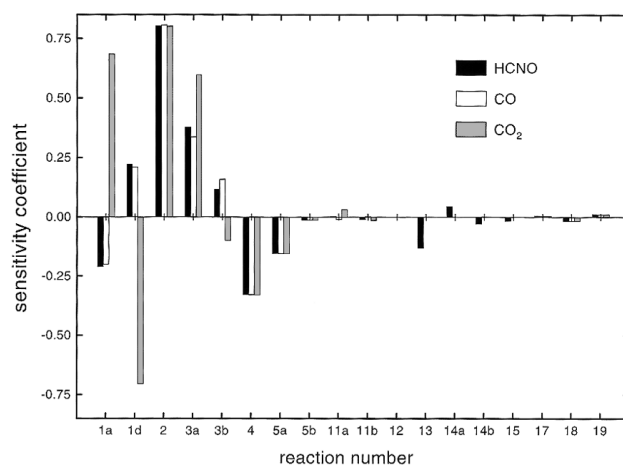


**Fig. 5** Sensitivity analysis for reaction mixture 10 (Table 1) after 40 min photolysis. The histograms show the reduced sensitivity coefficients  $\partial \ln c_i / \partial \ln k_j$  for the products HCNO, CO, and CO<sub>2</sub> with respect to variations of the rate constants of the main reactions in the mechanism of Table 3. Reactions omitted were found to have negligible sensitivity.

They also found mass signals at  $m/z = 43$ , consistent with a product with an "HCON" sum formula, which they attributed to HNCO. From the observed  $\text{CO}_2/\text{CO}$  ratio, and the alleged HNCO detection, reaction (1) was concluded to proceed according to channels (1a) and (1b) with  $k_{1a}/k_1 = 0.23$  and  $k_{1b}/k_1 = 0.77$ , respectively.

In an accompanying *ab initio* quantum chemical study, Nguyen *et al.*<sup>10</sup> derived stationary points and transition states on the HCCO + NO potential-energy surface. Assuming the reaction to proceed *via* an HC(NO)CO association complex (nitrosoketene), an exit channel was indeed found for the formation of HCN +  $\text{CO}_2$ , following isomerization of the HC(NO)CO complex *via* a four-centre cyclic transition state. However, the mechanism for the alleged production of HNCO remained very unclear. On the other hand, CO bond rupture in the HC(NO)CO complex to form HCNO + CO was found to be feasible. We mention here that different isomeric  $m/z = 43$  species, in particular HNCO and HCNO, cannot easily be distinguished in mass spectrometric work such as that of Boullart *et al.*<sup>9</sup> A reassignment of their  $m/z = 43$  mass signal to HCNO would bring their data into excellent agreement with the present results.

Miller *et al.*<sup>17</sup> very recently reported modelling calculations of the product distribution of reaction (1). Taking the *ab initio* potential-energy data for the system of Nguyen *et al.*,<sup>10</sup> they employed unimolecular rate theory to predict HCN +  $\text{CO}_2$  to be the major products (*ca.* 80%) at room temperature. HCNO + CO was calculated to account for the remaining *ca.* 20% of the reaction. With increasing temperature, the yield of HCN +  $\text{CO}_2$  was calculated to decrease and the production of HCNO + CO was found to increase. Other product channels were concluded to be negligible. These model calculations contrast with the experimental results, both of the present work and of Boullart *et al.*,<sup>9</sup> which show the dominance of the HCNO + CO channel. The discrepancy may be traced back to the calculated *ca.* 50 kJ mol<sup>-1</sup> energy difference between the rate-determining transition states for the two channels of interest on the potential surface of Nguyen *et al.*<sup>10</sup> According to Nguyen *et al.*, the HCN +  $\text{CO}_2$  channel is the energetically favoured one. It remains to be seen to what extent the calculated product branching ratio for reaction (1) is affected by small errors in the calculated transition state energies<sup>10</sup> and existing small deficiencies in the unimolecular rate theory model calculations of ref. 17.

Preparation of nitrosoketene *via* pyrolysis of isonitroso Meldrum's acid was reported by Matsui *et al.*<sup>34</sup> Their identification was based on FTIR spectra attributed to the HC(NO)CO molecule, on the grounds of quantum chemical IR frequency calculations. The assignment was supported by mass spectrometric observations using chemical ionization of an  $m/z = 72$  species, considered as HC(NO)CO · H<sup>+</sup>, and detection of a nitrosoketene dimer. Considering, however, the calculated low potential-energy barriers for the HC(NO)CO isomerization and decomposition reactions of Nguyen *et al.*,<sup>10</sup> the observation of a stable HC(NO)CO appears rather questionable. Several more stable isomers of HC(NO)CO exist<sup>10</sup> which may exhibit similar IR transitions.

We note that Matsui *et al.* did find a thermal decomposition of their product to HCNO + CO, which would be in agreement with our product observations.<sup>34</sup> On the other hand, they did not detect HCN. Depending on the energy barriers, the thermal decomposition of HC(NO)CO may yield products in different ratios than those from the energized HCCO + NO adduct.

#### 4.4 Implications for NO<sub>x</sub> reburning

NO<sub>x</sub> is generated as a pollutant in the combustion of hydrocarbons according to the well known Zeldovich, Fenimore, fuel-N, and N<sub>2</sub>O mechanisms (see *e.g.* ref. 35). The fast reac-

tion between HCCO and NO (1), as well as the reactions of CH<sub>3</sub>, CH<sub>2</sub>, and CH with NO, are of fundamental importance because they lead to recycling of the NO back into the reaction mechanism. These reactions have found technical importance in the so-called reburn stages in large-scale power generation (*e.g.* ref. 35).

Reaction (1) has been proposed as the main NO reburning reaction under some fuel-rich conditions.<sup>5,6</sup> The detailed NO reduction routes, and thus all NO reburn models, are, however, highly critically affected by branching between the  $\text{CO}_2$  + HCN and the HCNO + CO channels (1a) and (1d). The conversion of NO to HCN is a key step in the NO reburn mechanism.<sup>5,36,37</sup> HCN is subsequently converted to NH<sub>i</sub> and N<sub>2</sub> under rich conditions.<sup>1,3</sup> The HCNO could isomerize to HNCO which would again lead to NH<sub>i</sub> (HNCO has been suggested as an additive for selective NO reduction according to the Rapreox process<sup>38</sup>). On the other hand, the recent model calculations by Miller *et al.* suggest that fast bimolecular reactions of HCNO with OH and O lead to rapid regeneration of the NO.<sup>17</sup>

A number of research groups have been involved in modelling laboratory-scale plug flow reactor measurements of NO reburning (*e.g.* ref. 6, 15–17 and 39). Comprehensive mechanisms, as proposed especially by Glarborg *et al.*<sup>15</sup> (GADM), Bockhorn *et al.*<sup>37</sup> (DCWW), the Gas Research Institute<sup>40</sup> (GRI), and Dean and Bozelli<sup>41</sup> (DB), have formed the basis for the modelling. Critical importance was attributed to the formation of HCN, which was used to assess the different models. In a comparative study, Schelb *et al.*<sup>39</sup> observed that the HCN profiles under rich conditions were described by the GADM mechanism. However, the GADM mechanism adopted reaction (1a) as a major NO reburn step. Furthermore, Glarborg and Miller<sup>15–17</sup> were unsuccessful in modelling similar plug flow reactor NO reburn measurements of HCN assuming HCNO + CO as the main products of HCCO + NO. It appears that the formation of HCN in NO reburning still requires further investigation.

Extrapolation of our data to higher temperatures depends on the tightness and on the relative energies of the transition states. On the one hand, reaction (1a) is thought to have a tighter transition state than reaction (1d) which would favour HCNO + CO over HCN +  $\text{CO}_2$  as the dominating higher-temperature products. On the other hand, HCN +  $\text{CO}_2$  would be expected to increase compared to HCNO + CO if the energy barrier for reaction (1a) was higher than that for reaction (1d). At typical reburn temperatures, given the available data, both channels are likely to contribute. Further computational work on reaction (1), in which we will address the question of the temperature dependence by unimolecular rate theory, is currently underway (see also ref. 17). In any case, the title reaction is seen to have substantial effect on the NO to HCN conversion rate in the NO<sub>x</sub> reburn process.

It becomes obvious that major questions regarding the detailed elementary reaction steps in the NO reburn mechanism still remain to be answered.

## 5 Conclusions

In the present work, the reaction HCCO + NO was found to proceed according to two major channels,



From FTIR measurements of the  $\text{CO}_2$ , CO, and HCNO, the branching ratios are  $k_{1a}/k_1 = (0.28 \pm 0.10)$  and  $k_{1d}/k_1 = (0.64 \pm 0.12)$  for room temperature and up to *ca.* 1 bar pressure.

The advantage of the FTIR technique used is its unique versatility, this was instrumental for the detection of HCNO, but this versatility was bought at the expense of time

resolution. Time-resolved direct measurements of reaction (1) would, therefore, be of great interest to support the present findings. With the recent detection of HCCO with laser induced fluorescence,<sup>42</sup> and with the advent of stable, low-cost single-mode tunable diode lasers in the near-IR, real-time experiments with sensitive direct detection of HCNO and HCN do indeed appear feasible. HCNO is known to exhibit a very rich near-IR spectrum.<sup>43</sup> Furthermore, interest arises in the unimolecular isomerization of HCNO to HNCO and in the kinetics of bimolecular reactions of HCNO with small radicals like OH, O, or H.

## Acknowledgements

This work has been supported by the Deutsche Forschungsgemeinschaft within SFB 357 (Molekulare Mechanismen Unimolekularer Prozesse) and by the Fonds der Chemischen Industrie. We thank Dr. J. Gripp for the preparation of the HCNO reference sample.

## References

- J. O. L. Wendt, C. V. Sternling and M. A. Matovich, *14th International Symposium on Combustion*, The Combustion Institute, Pittsburgh, 1972, p. 897.
- S. L. Chen, J. M. McCarthy, W. D. Clark, M. P. Heap, W. R. Seeker and D. W. Pershing, *21st International Symposium on Combustion*, The Combustion Institute, Pittsburgh, 1988, p. 1159.
- T. Kolb, P. Jansohn and W. Leuckel, *22nd International Symposium on Combustion*, The Combustion Institute, Pittsburgh, 1989, p. 1193.
- T. Etzkorn, S. Muris, J. Wolfrum, C. Dembny, H. Bockhorn, P. F. Nelson, A. Attia-Shahin and J. Warnatz, *24th International Symposium on Combustion*, The Combustion Institute, Pittsburgh, 1992, p. 925.
- J. A. Miller and C. T. Bowman, *Progr. Energy Sci. Combust.*, 1989, **15**, 287.
- D. Stapf and W. Leuckel, *26th International Symposium on Combustion*, The Combustion Institute, Pittsburgh, 1996, p. 2083.
- K. G. Unfried, G. P. Glass and R. F. Curl, *Chem. Phys. Lett.*, 1991, **177**, 33.
- F. Temps, H. Gg. Wagner and M. Wolf, *Z. Phys. Chem.*, 1992, **176**, 27.
- W. Boullart, M. T. Nguyen and J. Peeters, *J. Phys. Chem.*, 1994, **98**, 8036.
- M. T. Nguyen, W. Boullart and J. Peeters, *J. Phys. Chem.*, 1994, **98**, 8030.
- Thermodynamic data from ref. 12 and 13, except for  $\Delta_f H_{298}^\circ(\text{HCCO}) = +177 \text{ kJ mol}^{-1}$  from ref. 14.
- R. Atkinson, D. L. Baulch, R. A. Cox, R. F. Hampson Jr., J. A. Kerr, M. J. Rossi and J. Troe, *J. Phys. Chem. Ref. Data*, 1997, **26**, 521.
- C. F. Melius, *BAC-MP4 Heats of Formation and Free Energies*, Sandia National Laboratories, Livermore, 1990.
- D. L. Osborn, D. H. Mordaut, H. Choi, R. T. Bise, D. M. Neumark and C. M. Rohlfing, *J. Chem. Phys.*, 1997, **106**, 10087.
- P. Glarborg, M. U. Alzueta, K. Dam-Johansen and J. A. Miller, *Combust. Flame*, 1998, in press.
- L. Prada and J. A. Miller, *Combust. Sci. Tech.*, 1998, in press.
- J. A. Miller, J. L. Durant and P. Glarborg, *27th International Symposium on Combustion*. The Combustion Institute, Pittsburgh, 1998, in press.
- J. Grußdorf, F. Temps and H. Gg. Wagner, *Ber. Bunsen-Ges. Phys. Chem.*, 1997, **101**, 134.
- C. Wentrup, B. Gerecht and H. Briehl, *Angew. Chem.*, 1979, **91**, 503; G. Schulze, Diploma Thesis, Gießen, 1993.
- Z. Vecera and P. N. Dasgupta, *Environ. Sci. Technol.*, 1991, **25**, 255; P. Pagsberg, E. Ratajczak, A. Sillesen and Z. Latajka, *Chem. Phys. Lett.*, 1994, **227**, 6.
- E. L. Feretti and K. N. Rao, *J. Mol. Spectrosc.*, 1974, **51**, 97.
- A. B. Harker and H. J. Johnston, *J. Phys. Chem.*, 1973, **77**, 1153.
- H. Gaedke and J. Troe, *Ber. Bunsen-Ges. Phys. Chem.*, 1975, **79**, 184.
- J. Hahn, Diploma Thesis, Göttingen, 1998.
- J. V. Michael, W. A. Payne and D. A. Whytock, *J. Chem. Phys.*, 1976, **65**, 4830; G. Yarwood, J. W. Sutherland, M. A. Wickramaaratchi and R. B. Klemm, *J. Phys. Chem.*, 1991, **95**, 8771.
- J. Peeters, M. Schaekers and C. Vinckier, *J. Phys. Chem.*, 1986, **90**, 6552; W. Boullart and J. Peeters, *J. Phys. Chem.*, 1992, **96**, 9810; J. Peeters, W. Boullart and I. Langhans, *Int. J. Chem. Kinet.*, 1994, **26**, 869; J. V. Michael and A. F. Wagner, *J. Phys. Chem.*, 1990, **94**, 2453.
- U. Bley, M. Koch, C. Oehlers, F. Temps and H. Gg. Wagner, *23rd International Symposium on Combustion*, Abstract P-105, Orleans, 1990.
- D. L. Baulch, C. J. Cobos, R. A. Cox, C. Esser, P. Frank, Th. Just, J. A. Kerr, M. J. Pilling, J. Troe, R. W. Walker and J. Warnatz, *J. Phys. Chem. Ref. Data*, 1992, **21**, 411; D. L. Baulch, C. J. Cobos, R. A. Cox, P. Frank, G. Hayman, Th. Just, J. A. Kerr, T. Murrells, M. J. Pilling, J. Troe, R. W. Walker and J. Warnatz, *J. Phys. Chem. Ref. Data*, 1994, **23**, 847.
- W. G. Mallard, F. Westley, J. T. Herron, R. F. Hampson and D. H. Frizzell, NIST Chemical Kinetics Database, Ver. 5.0, NIST Standard Reference Data, Gaithersburg, MD, 1993.
- V. Seidler, F. Temps, H. Gg. Wagner and M. Wolf, *J. Phys. Chem.*, 1989, **93**, 1070.
- T. Böhland, F. Temps and H. Gg. Wagner, ref. 2, p. 841.
- J. J. Ahumada, J. V. Michael and D. T. Osborne, *J. Chem. Phys.*, 1972, **57**, 3736.
- A. B. Callear and R. W. Carr, *J. Chem. Soc., Faraday Trans. 2*, 1975, **71**, 1603; Y. He and M. C. Lin, *Int. J. Chem. Kinet.*, 1992, **24**, 743.
- H. Matsui, E. J. Zücker, N. Katagiri, C. Kaneko, S. Ham and D. M. Birney, *J. Phys. Chem.*, 1997, **101**, 3936.
- J. Warnatz, U. Maas and R. W. Dibble, *Combustion*, Springer, Berlin, 1998.
- P. Glarborg and S. Hadvig, *Development and Test of a Kinetic Model for Natural Gas Combustion*, Nordic Gas Technology Center, 1991.
- H. Bockhorn, Ch. Chevalier, J. Warnatz and V. Weyrauch, *VDI-Berichte*, 1991, **922**, 171.
- R. A. Perry and D. L. Siebers, *Nature (London)*, 1986, **342**, 657.
- D. Schelb, M. Braun-Unkloff, P. Frank, F. Lecomte, M. Cathonnet and Ph. Dagaut, *27th International Symposium on Combustion*, Poster W2B17, Boulder, CO, 1998.
- C. T. Bowman, R. K. Hanson, D. F. Davidson, W. C. Gardiner, V. Lisianski Jr., G. P. Smith, D. M. Golden, M. Frenklach and M. Goldenberg, GRI-MECH 2.11, [http://www.berkeley.me.edu/gri\\_mech](http://www.berkeley.me.edu/gri_mech), 1996.
- A. M. Dean and J. W. Bozelli, in *Combustion Chemistry II*, ed. W. C. Gardiner Jr., Springer, Berlin, 1998, in press.
- L. R. Brock, B. Mischler, E. A. Rohlfing, R. T. Bise and D. M. Neumark, *J. Chem. Phys.*, 1997, **107**, 665.
- S. Albert, M. Winnewisser and B. P. Winnewisser, *Ber. Bunsen-Ges. Phys. Chem.*, 1997, **101**, 1165.

Paper 8/07258B